Ionics (2009) 15:233–239
DOI 10.1007/s11581-008-0265-5

ORIGINAL PAPER

Enhanced cyclability of triple-metal-doped $LiMn_2O_4$ spinel as the cathode material for rechargeable lithium batteries

H. Göktepe · H. Şahan · Ş. Patat · A. Ülgen

Received: 7 May 2008 / Revised: 26 June 2008 / Accepted: 25 July 2008 / Published online: 23 August 2008

Abstract To improve the cycle performance of spinel $LiMn_2O_4$ as the cathode of 4-V-class lithium secondary batteries, spinel phases $LiM_xMn_{2-x}O_4$ (M=Li, Fe, Co; x=0, 0.05, 0.1, 0.15) and $LiFe_{0.05}M_yMn_{1.95-y}O_4$ (M=Li, Al, Ni, Co; y=0.05, 0.1) were successfully prepared using the sol–gel method. The spinel materials were characterized by powder X-ray diffraction (XRD), elemental analysis, and scanning electron microscopy. All the samples exhibited a pure cubic spinel structure without any impurities in the XRD patterns. Electrochemical studies were carried out using the $Li|LiM_xMn_{2-x}O_4$ (M=Li, Fe, Co; x=0, 0.05, 0.1, 0.15) and $LiFe_{0.05}M_yMn_{1.95-y}O_4$ (M=Li, Al, Ni, Co; y= 0.05, 0.1) cells. These cathodes were more tolerant to repeated lithium extraction and insertion than a standard $LiMn_2O_4$ spinel electrode in spite of a small reduction in the initial capacity. The improvement in cycling performance is attributed to the stabilization in the spinel structure by the doped metal cations.

Keywords Lithium-ion battery · Substituted $LiMn_2O_4$ · Oxide cathodes · Triple-metal doping · Electrochemical properties

Introduction

One of the recent trends in the lithium ion battery technology is focused on the characterization and development of high-voltage cathodes. Lithium transition-metal (V, Cr, Mn, Co, Ni) oxides, which are used as positive electrodes in secondary lithium batteries, have been extensively studied [1–4]. Among the various positive electrodes which have been used, spinel $LiMn_2O_4$ [5–7] offers considerable advantages over $LiCoO_2$ [8] and $LiNiO_2$ [9, 10] in terms of high cell voltage, a wide operating temperature, and long shelf life with much lower cost.

In spinel $LiMn_2O_4$, Li ions reside in the tetrahedral (8a) sites, Mn ions in the octahedral (16d) sites, and O^{2-} ions in octahedral (32e) sites, respectively [11]. The oxygen ions in the octahedral sites form a closed-packed array in the spinel structure. The tetrahedral (8a) sites share faces with empty octahedral (l6c) sites and thus form 3D spaces. Li ions intercalate or de-intercalate through these spaces during electrochemical reaction [12].

Some problems for commercial application of $LiMn_2O_4$ are rechargeable capacity and poor cyclability of the charge–discharge process in the 4-V region. The major factors responsible for the capacity loss are as follows [10, 13, 14]: (1) the more stable one-phase structure in the low-voltage region transforms to an unstable two phase on the high-voltage region; (2) Mn^{3+} ions in $LiMn^{3+}Mn^{4+}O_4$ cathode materials undergo a self-redox reaction to Mn^{2+} and Mn^{4+} at high voltages, which induces capacity loss due to a loss of the cathode; the Mn^{2+} so generated irreversibly dissolves in the electrolyte and increases in resistance of the cell; (3) the decomposition of the electrolyte solution at the electrode at high voltage causes lattice instability of $LiMn_2O_4$. This metal oxide shows cubic $Fd\bar{3}m$ symmetry at room temperature, with an average manganese valence of 3.5. The Mn exists in Mn^{4+} $\left(t_{2g}^3 e_g^0\right)$ and Jahn–Teller active Mn^{3+} $\left(t_{2g}^3 e_g^1\right)$ configurations. Several studies have been aimed at improving the material properties of $LiMn_2O_4$ and at improving its efficiency in maintaining electrochemical capacity over a large number of cycles without sacrificing

H. Göktepe · H. Şahan · Ş. Patat (✉) · A. Ülgen
Department of Chemistry, Faculty of Arts and Science,
Erciyes University,
38039 Kayseri, Turkey
e-mail: patat@erciyes.edu.tr

initial reversible capacity and also its performance at room temperature [15, 16]. Doping the Mn (16d) sites with a trivalent cation or a cation with lower valence is a possibility, because it reduces the Mn^{3+} content and stabilizes the cubic structure in the face of Mn^{3+} Jahn–Teller distortion [17–23]. Guohua et al. [22] have shown that the substitution of M ions at the Mn site, Li(Mn, M)$_2O_4$ (M=Cr, Co and Ni), increases the average ionic valence of Mn and thus decreases the number of Jahn–Teller Mn^{3+} ions. Thackeray and co-workers [24] have pointed out that the substitution of a metal cation for Mn enhances the stability of spinels. In addition, Hosoya et al. [25] have suggested that the improvement of the cyclability refers to stronger M–O bonding of the MO_6 octahedron of partially substituted $LiM_yMn_{2-y}O_4$ (M=Cr, Co, Ni) in comparison with that of Mn–O in the parent $LiMn_2O_4$. Single-ion-doped $LiMn_2O_4$ spinels could not counteract all the factors responsible for the capacity loss. The effect of multiple cation-substituted $LiMn_2O_4$ has been reported and it has been pointed out that co-doping has a synergistic effect on the improvement of the cycling life of the materials as cathodes in lithium batteries [26–31].

In this work, we report the synthesis and characterization of double- and triple-metal-cation-doped spinel phases, wherein Mn has been partially replaced with monovalent lithium and other metal ions to improve the cycle performance of $LiMn_2O_4$ spinel materials.

Experimental

The $LiM_xMn_{2-x}O_4$ (M=Li, Fe, Co; x=0, 0.05, 0.1, 0.15) and $LiFe_{0.05}M_yMn_{1.95-y}O_4$ (M=Li, Al, Ni, Co; y=0.05, 0.1) powders were synthesized by the sol–gel method using citric acid as a chelating agent [32, 33]. Stoichiometric mixture of $Mn(NO_3)_2{\cdot}4H_2O$ (Merck), $Fe(NO_3)_3{\cdot}9H_2O$ (Merck), and the respective substituent compound [$Al(NO_3)_3{\cdot}9H_2O$ (Riedel-de Haen), $Co(NO_3)_2{\cdot}6H_2O$ (Surechem), $Ni(NO_3)_2{\cdot}6H_2O$ (Merck)] was first dissolved in deionized water to give a saturated solution. To this solution, lithium nitrate (Riedel-de Haen) was added slowly with mild stirring. Finally, a saturated aqueous solution of citric acid was then added with stirring. In all the experiments, the molar ratio of chelating agent to the total metal ions was unity. The pH of the mixed solution was maintained between 6.5 and 7.0 by adding ammonium hydroxide solution. The solution was then heated at 80 °C with vigorous stirring for 4 h to remove excess ammonia and water. The resulting precipitate of metal citrate was dried in an air oven for 10 h at 100 °C. After drying, the precursors were decomposed at 300 °C for 6 h in air to eliminate organic contents. The decomposed powders were slightly ground and then calcined at 600–800 °C for 24 h in air.

The cation composition of the products was determined by flame atomic absorption spectrometer (AAS, Perkin Elmer 3110) after dissolving the powders in dilute nitric acid.

The valence of Mn was determined by chemical titration. The samples were dissolved in an excess of 20 ml $Na_2C_2O_4$ and 2 ml H_2SO_4 at ~65 °C (maintained by a water bath) to reduce all Mn^{n+} to Mn^{2+} ($2<n\leq4$), and then the excess $C_2O_4^{2-}$ ions in the solution were determined by titration at 65 °C with a standard solution of $KMnO_4$ [34].

The phase identification and the evaluation of lattice parameters of prepared samples were carried out by powder X-ray diffraction (XRD) using copper CuK_α radiation (Bruker AXS D8). The diffractometer was equipped with a diffracted beam graphite monochromator. The diffraction data were collected at 40 kV and 40 mA over a 2θ range from 5° to 80° with a step size of 0.02° and a count time of 10 s/step.

The particle morphology of the products was examined by means of scanning electron microscopy (LEO 440) operated at 20 kV.

The electrochemical properties of the spinel products were investigated using two-electrode Teflon cells [25] consisting of a cathode, lithium foil anode, glass filter paper separator, and an electrolyte having 1 M $LiClO_4$ in propylene carbonate. For the fabrication of the cathode, a mixture of 85 wt.% active material ($LiM_xMn_{2-x}O_4$ (M=Li, Fe, Co; x=0, 0.05, 0.1, 0.15) and $LiFe_{0.05}M_yMn_{1.95-y}O_4$

Table 1 Chemical analysis and average Mn oxidation state of $LiM_xMn_{2-x}O_4$ (M=Li, Fe, Co; x=0, 0.05, 0.1, 0.15) and $LiFe_{0.05}M_yMn_{1.95-y}O_4$ (M=Li, Al, Ni, Co; y=0.05, 0.1) compounds

Nominal composition	Experimental composition	Average oxidation state of Mn	
		Theoretical[a]	Experimental
$Li_{1.05}Mn_2O_4$	$Li_{1.01}Mn_{1.97}O_4$	3.55	3.55
$Li_{1.1}Mn_2O_4$	$Li_{1.05}Mn_{1.96}O_4$	3.55	3.53
$Li_{1.1}Fe_{0.05}Mn_{1.95}O_4$	$Li_{1.04}Fe_{0.049}Mn_{1.93}O_4$	3.53	3.53
$Li_{1.1}Fe_{0.1}Mn_{1.9}O_4$	$Li_{1.05}Fe_{0.0.96}Mn_{1.88}O_4$	3.54	3.54
$Li_{1.1}Co_{0.15}Mn_{1.85}O_4$	$Li_{1.03}Co_{0.145}Mn_{1.81}O_4$	3.69	3.67
$Li_{1.1}Fe_{0.05}Al_{0.1}Mn_{1.85}O_4$	$Li_{1.05}Fe_{0.048}Al_{0.098}Mn_{1.81}O_4$	3.60	3.57
$Li_{1.1}Fe_{0.05}Ni_{0.1}Mn_{1.85}O_4$	$Li_{1.05}Fe_{0.048}Ni_{0.098}Mn_{1.81}O_4$	3.65	3.65
$Li_{1.1}Fe_{0.05}Co_{0.1}Mn_{1.85}O_4$	$Li_{1.04}Fe_{0.049}Co_{0.097}Mn_{1.80}O_4$	3.67	3.68

[a] The theoretical oxidation state of Mn is calculated, based on the experimental composition

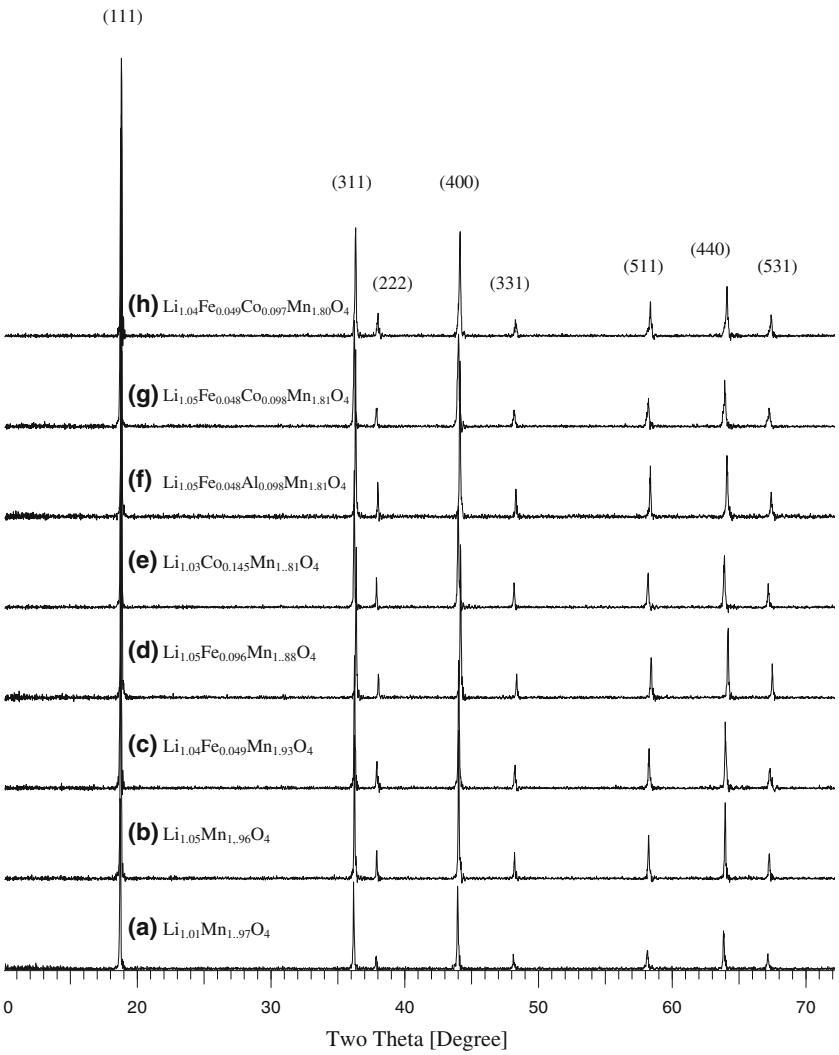

Fig. 1 X-ray diffraction patterns of $LiM_xMn_{2-x}O_4$ (*M*= Li, Fe, Co; x=0, 0.05, 0.1, 0.15) and $LiFe_{0.05}M_yMn_{1.95-y}O_4$ (M=Li, Al, Ni, Co; y=0.05, 0.1) powders. **a** $Li_{1.01}Mn_{1.97}O_4$, **b** $Li_{1.05}Mn_{1.96}O_4$, **c** $Li_{1.04}Fe_{0.049}Mn_{1.93}O_4$, **d** $Li_{1.05}Fe_{0..96}Mn_{1.88}O_4$, **e** $Li_{1.03}Co_{0.145}Mn_{1.81}O_4$, **f** $Li_{1.05}Fe_{0.048}Al_{0.098}Mn_{1.81}O_4$, **g** $Li_{1.05}Fe_{0.048}Ni_{0.098}Mn_{1.81}O_4$, **h** $Li_{1.04}Fe_{0.049}Co_{0.097}Mn_{1.80}O_4$

(M=Li, Al, Ni, Co; y=0.05, 0.1), 10 wt.% graphite as electronic conductor, and 5 wt.% PTFE as a binder was pressed on to a 13-mm-diameter stainless steel mesh current collector covered with aluminum foil under a pressure of 6 tons. The resulting disc was then dried at 120 °C under vacuum for 12 h. The charge–discharge tests were performed galvanostatically with a computer-controlled multichannel battery tester at a constant current density of 0.300 mA/cm^2 with cut-off potentials of 3.5–4.4 V versus Li/Li^+ at 25 °C. All processes of assembling and dismantling the cells were carried out in an argon-filled dry glove box.

Results and discussion

The chemical composition and the oxidation state of Mn in spinel materials are listed in Table 1. The chemical

Table 2 The cubic lattice parameter (a) and unit cell volume (V) for $LiM_xMn_{2-x}O_4$ (M=Li, Fe, Co; x=0, 0.05, 0.1, 0.15) and $LiFe_{0.05}M_yMn_{1.95-y}O_4$ (M=Li, Al, Ni, Co; y=0.05, 0.1)

Experimental composition	a (Å)	V (Å^3)
$Li_{1.01}Mn_{1.97}O_4$	8.2238	556.2
$Li_{1.05}Mn_{1.96}O_4$	8.2405	559.6
$Li_{1.04}Fe_{0.049}Mn_{1.93}O_4$	8.2229	556.0
$Li_{1.05}Fe_{0.96}Mn_{1.88}O_4$	8.2192	555.3
$Li_{1.03}Co_{0.145}Mn_{1.81}O_4$	8.1880	548.9
$Li_{1.05}Fe_{0.048}Al_{0.098}Mn_{1.81}O_4$	8.1998	551.3
$Li_{1.05}Fe_{0.048}Ni_{0.098}Mn_{1.81}O_4$	8.2189	555.2
$Li_{1.04}Fe_{0.049}Co_{0.097}Mn_{1.80}O_4$	8.2033	552.1

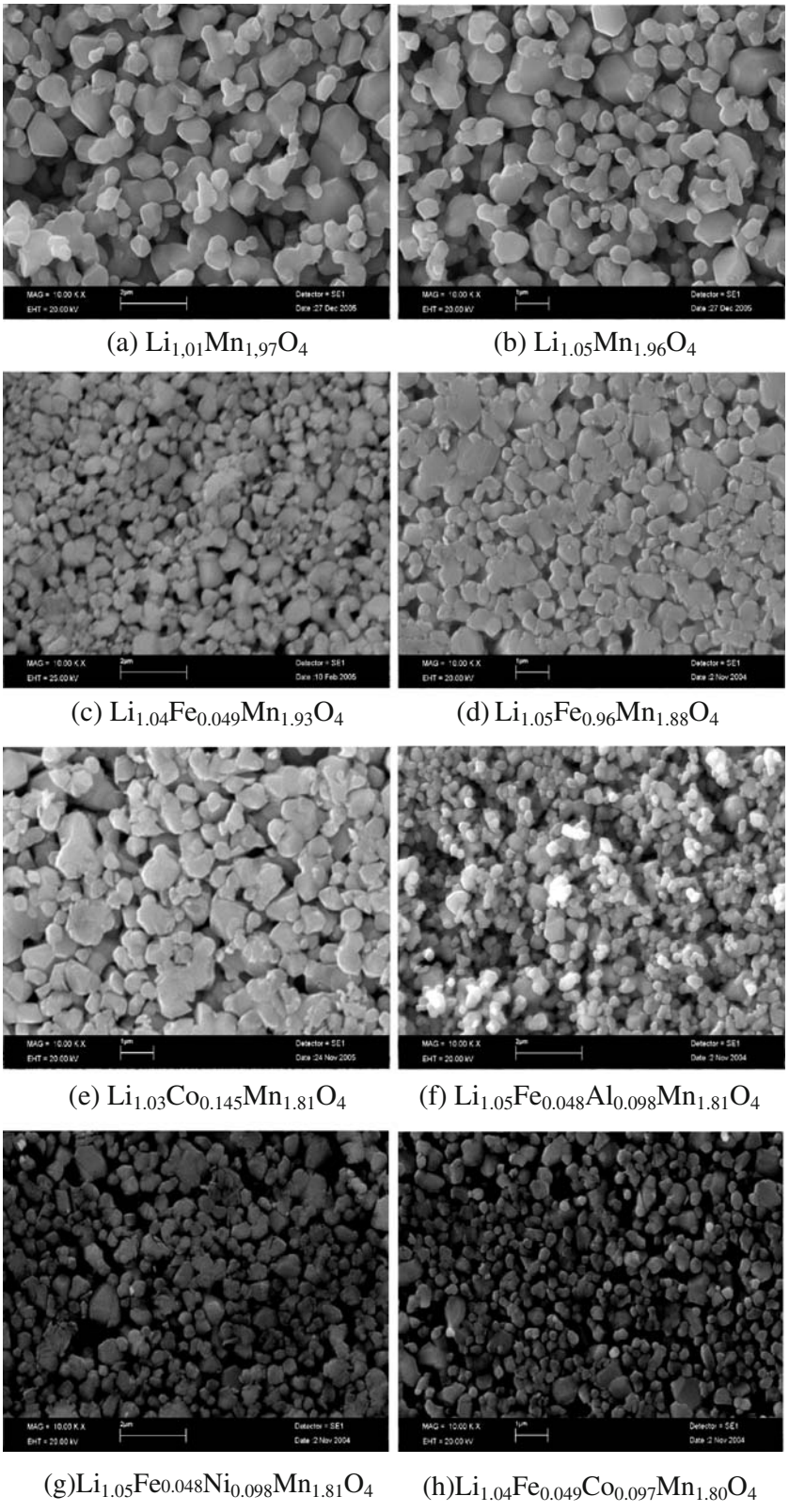

(a) $Li_{1,01}Mn_{1,97}O_4$ (b) $Li_{1.05}Mn_{1.96}O_4$

(c) $Li_{1.04}Fe_{0.049}Mn_{1.93}O_4$ (d) $Li_{1.05}Fe_{0.96}Mn_{1.88}O_4$

(e) $Li_{1.03}Co_{0.145}Mn_{1.81}O_4$ (f) $Li_{1.05}Fe_{0.048}Al_{0.098}Mn_{1.81}O_4$

(g)$Li_{1.05}Fe_{0.048}Ni_{0.098}Mn_{1.81}O_4$ (h)$Li_{1.04}Fe_{0.049}Co_{0.097}Mn_{1.80}O_4$

Fig. 2 Scanning electron micrographs of $LiM_xMn_{2-x}O_4$ (M=Li, Fe, Co; x=0, 0.05, 0.1, 0.15) and $LiFe_{0.05}M_yMn_{1.95-y}O_4$ (M=Li, Al, Ni, Co; y=0.05, 0.1) powders

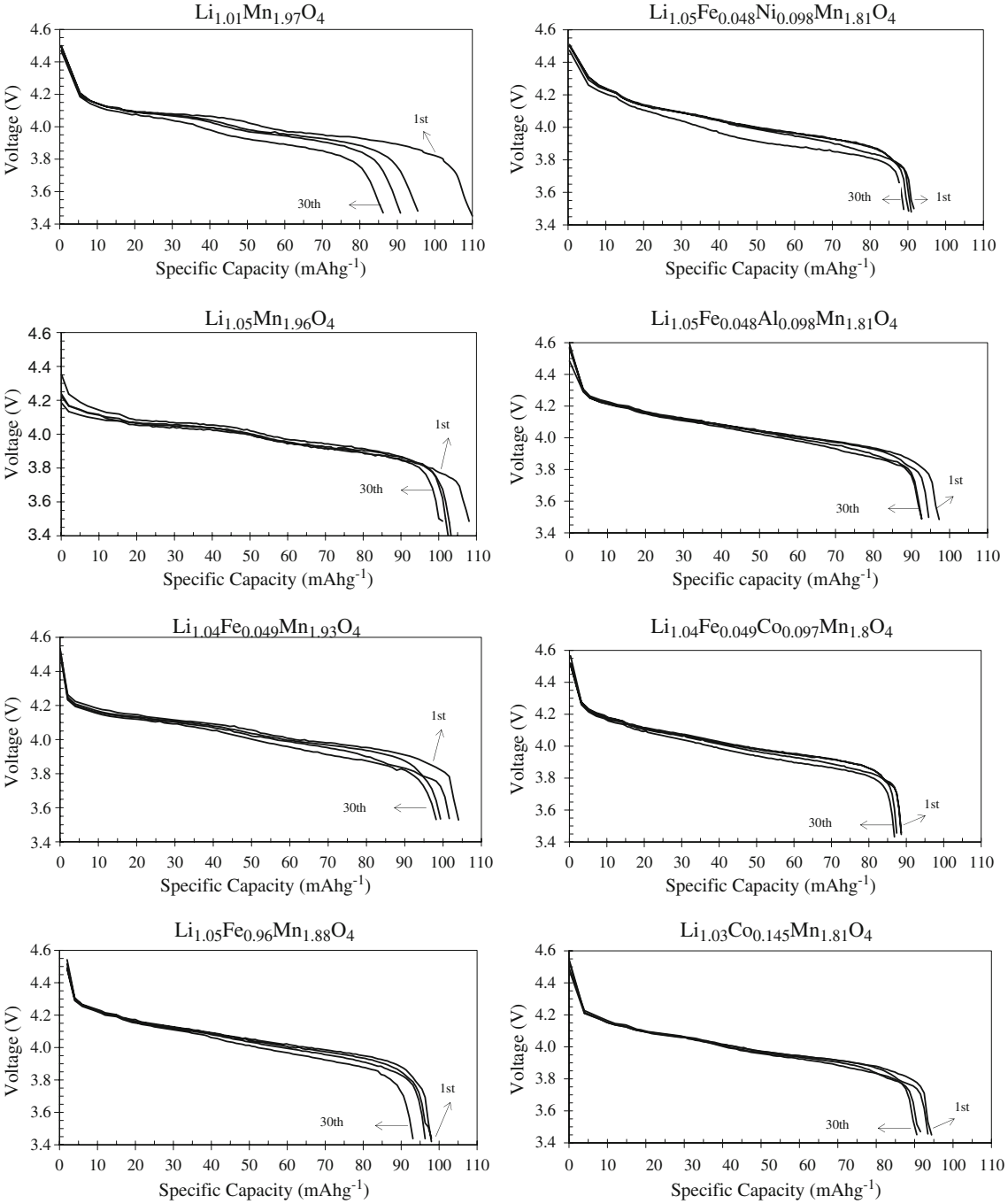

Fig. 3 Voltage vs. discharge capacity curves for various numbers of discharge cycles in voltage range 3.5–4.5 V at a current density of 0.3 mA cm^{-2} for Li/Li$M_xMn_{2-x}O_4$ (M=Li, Fe, Co; x=0, 0.05, 0.1, 0.15) and Li$Fe_{0.05}M_yMn_{1.95-y}O_4$ (M=Li, Al, Ni, Co; y=0.05, 0.1) cells

composition of each sample was close to the targeted formula of Li$M_xMn_{2-x}O_4$ (M=Li, Fe, Co; x=0, 0.05, 0.1, 0.15) and Li$Fe_{0.05}M_yMn_{1.95-y}O_4$ (M=Li, Al, Ni, Co; y= 0.05, 0.1). The experimental oxidation state of Mn was determined by chemical titration and the theoretical one is calculated based on the experimental composition. It can be seen that there is a good agreement between the expected and observed values.

The powder XRD patterns of the Li$M_xMn_{2-x}O_4$ (M=Li, Fe, Co; x=0, 0.05, 0.1, 0.15) and Li$Fe_{0.05}M_yMn_{1.95-y}O_4$ (M=Li, Al, Ni, Co; y=0.05, 0.1) are shown in Fig. 1. All samples were identified as a single-phase spinel with a space group *Fd3m* in which the lithium ions occupy the tetrahedral sites (8a) and manganese and substituting metal ions reside at the octahedral (16d) sites [12]. This fact may indicate that the Mn site in $LiMn_2O_4$ is substituted fully by

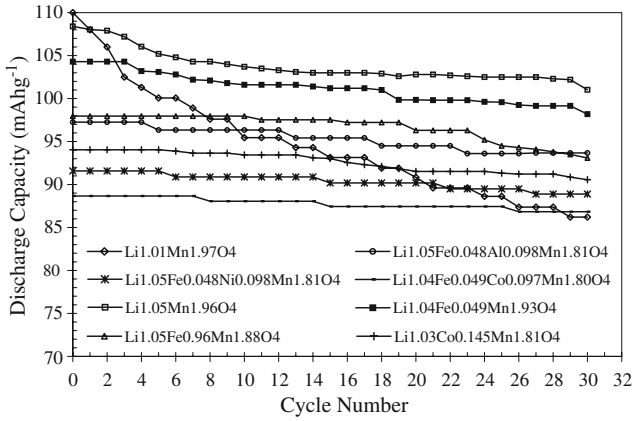

Fig. 4 Variation of discharge capacity as a function of cycle number for $Li/LiM_xMn_{2-x}O_4$ (M=Li, Fe, Co; x=0, 0.05, 0.1, 0.15) and $Li/LiFe_{0.05}M_yMn_{1.95-y}O_4$ (M=Li, Al, Ni, Co; y=0.05, 0.1) cells

Fe–, Al–, Ni–, and Co–, respectively, and no other phase is formed. Metal substitution does not appear to change the basic $LiMn_2O_4$ structure. The cubic lattice parameters of $LiM_xMn_{2-x}O_4$ (M=Li, Fe, Co; x=0, 0.05, 0.1, 0.15) and $LiFe_{0.05}M_yMn_{1.95-y}O_4$ (M=Li, Al, Ni, Co; y=0.05, 0.1), calculated from the diffraction data, are given in Table 2. As compared with that of $Li_{1.01}Mn_2O_4$, the lattice parameters of doped spinels are slightly decreased with increasing dopant content. This is due to the smaller size of the substituting ions Li^+ (0.059 nm), Al^{3+} (0.0535 nm), Co^{3+} (0.055 nm), and Fe^{3+} (0.064 nm) as compared with the larger Mn^{+3} ion (0.066 nm) [35].

SEM photographs of substituted spinel $LiM_xMn_{2-x}O_4$ (M=Li, Fe, Co; x=0, 0.05, 0.1, 0.15) and $LiFe_{0.05}M_yMn_{1.95-y}O_4$ (M=Li, Al, Ni, Co; y=0.05, 0.1) powders are presented in Fig. 2. The micrographs show that the particle size becomes smaller and the size distribution becomes much narrower with substituting of metal ions for the Mn^{3+}. The smallest particle size and narrowest particle size distribution are observed for the triple-doped spinels. Since electrochemical lithium intercalation and deintercalation are, in general, limited by the rate of diffusion, the surface morphology and particle size distribution are the important factors for cycling performance of the Li ion batteries. Smaller grain size and narrower particle size distribution can favor the lithium ion mobility in the particles by reducing the ion diffusion pathway [36]. Therefore, it is expected that triple-doped spinels can display better electrode properties.

The discharge profiles for the samples synthesized by sol–gel method are shown in Fig. 3. The cells were first activated by charging up to 4.4 V and then discharging to 3.5 V at room temperature. The initial discharge capacity of cells was reduced by doping. Since the deintercalation of Li^+ from the spinel structure must be electrically compensated by the oxidation of Mn^{3+} to Mn^{4+}, it suggests that even for the substituted spinel phases only the amount of Mn^{3+} contributes to the charge capacity. So the initial capacity of $LiM_xMn_{2-x}O_4$ (M=Li, Fe, Co; x=0, 0.05, 0.1, 0.15) and $LiFe_{0.05}M_yMn_{1.95-y}O_4$ (M=Li, Al, Ni, Co; y=0.05, 0.1) is limited by the initial amount of Mn^{3+} in the 16d sites [12].

The variation of discharge capacity as a function of cycle number for the $LiM_xMn_{2-x}O_4$ (M=Li, Fe, Co; x=0, 0.05, 0.1, 0.15) and $LiFe_{0.05}M_yMn_{1.95-y}O_4$ (M=Li, Al, Ni, Co; y=0.05, 0.1) electrodes is given in Fig. 4. In Table 3, the theoretical capacities C_0, the first discharge capacities C_1, the discharge capacities at n=30, C_{30}, and the percentages of capacity deterioration at the 30th cycle $(C_1-C_{30})\times 100/C_1$ under the standard of C_1 are summarized. As shown in Fig. 4 and Table 3, the initial discharge capacity of an electrode, based on $Li_{1.01}Mn_{1.97}O_4$, was 110 mAh/g, which decreased rapidly to 86.2 mAh/g after 30 cycles. The capacity loss observed with the $Li_{1.01}Mn_{1.97}O_4$ is about 21.6% after 30 cycles. The monovalent lithium ion- and other metal cation (M=Fe, Al, Ni, Co)-doped spinels display better cycle performance in terms of cycle life compared with $Li_{1.01}Mn_2O_4$. In addition, cycling performance in the double-doped spinels ($LiM_xMn_{2-x}O_4$ M=Li, Fe, Co; x=0, 0.05, 0.1, 0.15),

Table 3 Theoretical capacities C_0, first discharge capacities C_1, discharge capacities at n=30 C_{30}, and percentages of capacity deterioration at n=30 $(C_1-C_{30})\times 100/C_1$

Composition	C_0 (mAh/g)[a]	C_1 (mAh/g)	C_{30} (mAh/g)	$(C_1-C_{30})\times 100/C_1$ (%)
$Li_{1.01}Mn_{1.97}O_4$	149.1	110.0	86.2	21.6
$Li_{1.05}Mn_{1.96}O_4$	149.8	108.1	101.1	6.5
$Li_{1.04}Fe_{0.049}Mn_{1.93}O_4$	148.9	104.1	98.2	5.7
$Li_{1.05}Fe_{0.0.96}Mn_{1.88}O_4$	149.0	97.9	93.1	4.9
$Li_{1.03}Co_{0.145}Mn_{1.81}O_4$	150.0	94.1	90.3	4.0
$Li_{1.05}Fe_{0.048}Al_{0.098}Mn_{1.81}O_4$	152.3	97.3	93.7	3.7
$Li_{1.05}Fe_{0.048}Ni_{0.098}Mn_{1.81}O_4$	149.6	91.6	88.9	2.9
$Li_{1.04}Fe_{0.049}Co_{0.097}Mn_{1.80}O_4$	150.0	88.7	86.9	2.0

[a] Discharge capacity given by $[(nF)/(3.6M_W)]$, n=no. of Li^+ atoms inserted per formula unit, F=Faraday's constant (96,485 C mol^{-1}), M_W=molecular weight of intercalated compound

gradually decline; on the other hand, triple-doped spinels ($LiFe_{0.05}M_yMn_{1.95-y}O_4$ (M=Li, Al, Ni, Co; y=0.05, 0.1) exhibit better capacity retention on cycling.

The significant improvement in the cycle performance can be explained by postulating that the doped metal ions enhance the stability of the octahedral sites in spinel skeleton structure because the bonding energy of doped metal oxygen Al–O, Ni–O, and Co–O is stronger than that of Mn–O [22, 37, 38]. Therefore, the spinel structure becomes more tolerant to repeated charge–discharge by doping of Li–Fe–Al, Li–Fe–Ni, and Li–Fe–Co. From the analysis of our results and those of earlier reports, we suggest that the Jahn–Teller distortion caused by Mn^{3+} was suppressed by the partial metal substitution. Another reason for the decreased capacity fade for the double- and triple-doped spinel materials is a result of their reduced particle size compared to that for the single-doped and undoped $LiMn_2O_4$ spinels. It has been known that a decrease in the mean particle size has increased the cyclability of the cathode material since the mechanical stability of small particles is more than that of large particles [39, 40]. From Fig. 4, it can be seen that the cycle performance was increased with triple-metal substitution.

Conclusions

The $LiM_xMn_{2-x}O_4$ (M=Li, Fe, Co; x=0, 0.05, 0.1, 0.15) and $LiFe_{0.05}M_yMn_{1.95-y}O_4$ (M=Li, Al, Ni, Co; y=0.05, 0.1) have been prepared by the sol–gel method. All of the powders were identified as a single spinel phase with *Fd3m* space group. It has been demonstrated that cathodes based on substituting a part of Mn with Li–Fe–Al, Li–Fe–Ni, and Li–Fe–Co have good cycle life in spite of decrease in initial capacity. The improvement in cycling properties might be attributed to stabilization of spinel structure. Triple doping seems to have a synergetic effect on the improvement of the cycling life.

Acknowledgments This study was financially supported by the Research Foundation of Erciyes University (Kayseri, Turkey). The authors thank Mr. I. Akşit for the SEM observation.

References

1. Tarascon JM, Guyomard D (1993) Electrochimica Acta 38:1221
2. Winter M, Besenhard JO, Spahr ME, Novak P (1998) Adv Mater 10:725
3. Aurbach D (2000) J Power Sources 89:206
4. Scrosati B, Panero S, Reale P, Satolli D, Aihara Y (2002) J Power Sources 105:161
5. Thackeray MM, Kock A, Rossouw MH, Liles D, Bittihn R, Hoge D (1992) J Electrochem Soc 139:363
6. Tarascon JM, Wang E, Shokoohi FK, Mckinnon WR, Colson S (1991) J Electrochem Soc 138:2859
7. Pasquier A, Blyr A, Cressent A, Lenain C, Amatucci G, Tarascon JM (1999) J Power Sources 81–82:54
8. Reimers JN, Dahn JR (1992) J Electrochem Soc 139:2091
9. Ohzuku T, Ueda A, Nagayama M (1991) J Electrochem Soc 140:1862
10. Prado G, Fournes L, Delmas C (2000) Solid State Ion 138:19
11. Pistoia G, Zane D, Zhang Y (1995) J Electrochem Soc 142:2551
12. Wakihara M (2001) Mater Sci Eng R33:109
13. Xia Y, Kumada N, Yoshio M (2000) J Power Sources 90:135
14. Mukerje S, Thurston TR, Jisrawi MN, Yang XQ, McBreen J, Daroux ML, Xing XK (1998) J Electrochem Soc 145:466
15. Liu W, Kowal K, Farrington GC (1998) J Electrochem Soc 145:459
16. Miura K, Yamada A, Tanaka M (1996) Electrochimica Acta 41:249
17. Robertson AD, Lu SH Averill WF, Howard WF (1997) J Electrochem Soc 144:3500
18. Robertson AD, Lu SH, Averill WF, Howard WF (1997) J Electrochem Soc 144:3505
19. Pistoia G, Antonini A, Rosati R, Bellitto C, Ingo GM (1997) Chem Mater 9:1443
20. Ein-Eli Y, Howard WF Jr. (1997) J Electrochem Soc 144:L205
21. Sanchez L, Tirado JL (1997) J Electrochem Soc 144:1939
22. Guohua L, Ikuta H, Uchida T, Wakihara M (1996) J Electrochem Soc 143:178
23. Pasquier AD, Blyr A, Courjal P, Larcher D, Amatucci B, Tarascon JM (1999) J Electrochem Soc 146:428
24. Gummow RJ, Kock A, Thackeray MM (1994) Solid State Ion 69:59
25. Hosoys M, Ikuta H, Wakihara M (1998) Solid State lonics 111:153
26. Bonino F, Panero S, Satolli D, Scrosati B (2001) J Power Sources 97–98:389
27. Hwang BJ, Santhanam R, Hu SG (2002) J Power Sources 108:250
28. Manuel Stephan A, Renganathan NG, Gopukumar S, Subramanian V, Bobba R (2004) Solid State Ion 175:291
29. Alcantara R, Jaraba M, Lavela P, Lloris JM, Perez Vicente C, Tirado JL (2005) J Electrochem Soc 152:A13
30. Rojas RM, Amarilla JM, Pascual L, Rojo JM, Kovacheva D, Petrov K (2006) J Power Sources 160:529
31. Şahan H, Göktepe H, Patat Ş (2008) Inorganic Materials 44:420
32. Hwang BJ, Santhanam R, Liu DG (2001) J Power Sources 101:86
33. Hwang BJ, Santhanam R, Liu DG, Tsai YW (2001) J Power Sources 102:326
34. Hong YS, Han H, Kim K, Campet G, Choy H (2001) Solid State Ion 139:75
35. Taniguchi I (2005) Mater Chem Phys 92:172
36. Julien CM, Zaghib K (2004) Electrochimica Acta 50:411
37. Sun YK, Oh B, Lee HJ (2000) Electrochimica Acta 46:541
38. Myung ST, Komaba S, Kumagai N (2001) J Electrochem Soc 148:A482
39. Manev V, Ebner W, Thompson W, Dow S (1999) US Patent 5961949
40. Choi HJ, Lee KM, Kim GH, Lee JG (2001) J Am Ceram Soc 84:242